Hindawi
Journal of Nanomaterials
Volume 2019, Article ID 9686913, 12 pages
https://doi.org/10.1155/2019/9686913

Research Article

Effect of Size on the Saturable Absorption and Reverse Saturable Absorption in Silver Nanoparticle and Ultrafast Dynamics at 400 nm

Sandeep Kumar Maurya,[1] Anuradha Rout,[1] Rashid A. Ganeev,[1] and Chunlei Guo[1,2]

[1]*The Guo China-US Photonics Laboratory, State Key Laboratory of Applied Optics, Changchun Institute of Optics, Fine Mechanics and Physics, Chinese Academy of Sciences, Changchun 130033, China*
[2]*The Institute of Optics, University of Rochester, Rochester, NY 14627, USA*

Correspondence should be addressed to Chunlei Guo; guo@ciomp.ac.cn

Received 2 April 2019; Accepted 20 May 2019; Published 13 June 2019

Academic Editor: Bo Tan

Saturable absorption and reverse saturable absorption play an important role in the studies of the nonlinear optical properties of nanoparticles at resonant excitation. With this viewpoint, nonlinear absorption processes of chemically prepared silver nanoparticles in deionized water were studied using femtosecond laser pulses at 400 nm. Our nonlinear absorption study shows that there is competition between saturable absorption and two-photon absorption in prepared Ag NPs which depends on the size of the nanoparticles. We have also studied the ultrafast dynamics associated with nanoparticles which also results in the direct correlation between the ultrafast timescale and the size of the nanoparticle. The excitation of Ag NPs at 400 nm has shown the manifestation of damped oscillation which is attributed to the radial breathing mode oscillation due to acoustic vibration.

1. Introduction

Metal nanoparticles (NPs) have shown unique nonlinear optical (NLO) properties toward their potential application in various fields such as biomedicine [1–3], electronics [4, 5], information storage [6, 7], and sensing [8–10]. This is because of the appearance of the surface plasmon resonance (SPR) due to the reduced dimensionality responsible for the enhanced third-order optical nonlinearities. Several noble metal NPs have been studied under various conditions imposed by the intense light source [11–13].

Several groups have shown the behavior of metal NPs upon interaction with intense laser pulses [14–22]. Their studies show that different mechanisms are responsible for their NLO properties, which include saturable absorption (SA), two-photon absorption (2PA), optical limiting (OL), and optical Kerr nonlinearities. SA has a profound influence on the overall nonlinear optical response at sufficiently high power of the employed laser pulse [23]. Another phenomenon called reverse saturable absorption (RSA) [17, 24, 25] may counteract the absorption saturation processes. The RSA process occurs as a result of large absorption by the nonlinear absorber at high laser energy via excited state absorption because of the depletion of the ground state with the increase of the incident laser energies. The performance of such nonlinear materials is limited by the accompanying linear absorption at low input energy. In this case, the incident photons may be further absorbed by excited states when their population gets large enough in an excited state. These processes depend not only on the intensity of the incident photon but also on the frequency of the incident photon which plays an important role in their NLO properties depending on the resonant or nonresonant transitions. There are few reports on the competitive behavior of SA and RSA together due to the associated energy level of metal NPs,

which provide the possibility to be investigated with the variation of the size of NPs [8, 26].

Apart from NLO properties of materials, many-body interactions in a condensed matter and molecular system have been of great concern because the properties like electrical and thermal conduction, superconductivity through Raman scattering, and polaron formation are highly affected by an ultrafast process such as electron-phonon interactions [27–29]. It is found that the ultrafast process affects the electrical, thermal, and optical properties of bulk materials. Numerous efforts have been made and are still ongoing to understand the mechanism governing these ultrafast processes. There has been a great advancement to understand the role of electron-phonon interaction on the properties of reduced dimensional systems [30]. A vast literature is presented on electron-phonon interaction in NPs [31]. The interaction of NPs with short laser pulses undergoes various ultrafast processes such as electron-electron coupling, electron-phonon coupling, and phonon-phonon coupling. Apart from these ultrafast processes, various studies have focused on the dissipation of the acoustic vibrations in noble NPs upon ultrafast laser pulse excitation which is based on the size, shape, and surrounding mediums [31, 32].

Among various metal NPs, silver (Ag) NPs pose unique optoelectronic and thermal properties which lead to efficient use in a wide range of technological advancements such as molecular diagnostics and photonic devices based on its optical properties [33, 34]. Ag NPs exemplify amazingly efficient optical properties, which depend on the size and the shape of the particle. There have been several reports on the presence of SA and TPA in Ag NPs depending on the excitation wavelength [35–38]. At the same time, Ag NPs have been studied in order to observe ultrafast dynamics depending on their size and shape [39–41]. However, there are few reports on a systematic study in ultrafast dynamics associated with coherent oscillations depending on the size and shape of Ag NPs [42, 43]. Thus, our objective was to investigate the NLO properties and ultrafast dynamics associated with Ag NPs under SPR which can effectively provide the correlation of NLO properties and ultrafast dynamics with the size of NPs.

In this paper, we present the results of systematic studies of the chemically prepared Ag NPs which can efficiently provide the variation in the size of NPs. We demonstrate the impact of the size of Ag NP on the SA and RSA using femtosecond pulses at 400 nm and 800 nm. Ultrafast dynamics of chemically prepared Ag NPs is studied using femtosecond 400 nm. We observed the presence of acoustic vibration in Ag NPs upon excitation with the resonant wavelength. The effect of the size of NPs on acoustic oscillations and associated damping time constants was discussed in detail.

2. Experiments

2.1. Ag NP Preparation. In this study, Ag NPs were prepared by chemical reduction of sodium nitrate ($AgNO_3$) from sodium borohydride (SBH) in an aqueous medium. In order to prepare Ag NPs in deionized water, first, 0.043 g $AgNO_3$ was dissolved in 50 mL deionized water, and 0.012 g SBH was dissolved in 150 mL deionized water, respectively, with constant stirring for 30 min. 3 mL of aqueous $AgNO_3$ solution was dripped slowly into 10 mL of aqueous SBH solution at three different temperature conditions of 0°C, 25°C, and 60°C. This mixture was stirred for a few seconds, which allowed $AgNO_3$ and $NaBH_4$ to react completely. With the addition of $AgNO_3$, the solution gradually turned yellow, light gray, and dark gray which indicates that Ag NPs were formed. From here onward, we represent Ag NP suspensions as S1, S5, and S9 prepared by addition of $AgNO_3$ solution to SBH solution through the dripping method at 0°C, 25°C, and 60°C, respectively, whereas NP suspensions represented as S3, S7, and S11 were prepared by fast mixing of $AgNO_3$ and SBH solution at 0°C, 25°C, and 60°C, respectively. Thus, the Ag NPs prepared by these methods yield different sizes of the NPs. Prepared Ag NPs were characterized by a UV-Visible spectrometer (Cary Series, Agilent Technologies) and a scanning electron microscope (SEM, Hitachi S-4800).

Under the assumption that the optimal packing efficiency of Ag atoms under spherical NPs was estimated to be 74%, the concentration of Ag NP suspension was calculated by using the mean sizes of Ag NPs measured from respective SEM images. The concentrations of NP suspensions were determined to be 1.7, 2.4, 1.6, 2.4, 1.7, and 2 nmol/L for S1, S3, S5, S7, S9, and S11, respectively. The synthesized Ag NP suspensions were found to be stable up to 30 days which were confirmed by their UV-Visible spectroscopy measurements and SEM images. NLO studies were performed at low and high concentrations of Ag NP suspension. The change of the Ag NP concentration in deionized water was achieved through the dilution of synthesized Ag NPs using deionized water as a solvent.

2.2. Z-Scan Setup. A conventional technique [44, 45] was employed to study the NLO properties of the prepared Ag NPs in deionized water. Schematic of the experimental setup is shown in Figure 1(a). The pulse width of laser pulses at 800 and 400 nm was kept at 35 fs. 400 mm focal length lens were used to focus the laser pulse into the quartz cuvette containing NPs. We employed an open aperture scheme for determination of nonlinear optical parameters, like absorption saturation intensity and 2PA coefficient. The transmittance from the sample was obtained by moving the sample cuvette across the focal plane of the plano-convex lens along the beam propagation direction. The motorized translational stage was used to change the sample position with respect to the focal position of the lens, which is interfaced with a computer through the EPS301 motion controller. The transmitted beam after the sample was collected by a large area detector (silicon photodiode, Thorlabs PDA100A-EC) to ensure the collection of the full beam after passing through the sample cell. We fitted the experimental data with the following equations for the determination of SA and TPA coefficients:

$$T_{\mathrm{SA}} = 1 + \frac{I_0}{I_{\mathrm{sat}}\left(1 + Z^2/Z_0^2\right)}, \tag{1}$$

$$T_{\mathrm{TPA}}(z) = q^{-1} \times 1\mathrm{n}(1+q), \tag{2}$$

where $q = \beta I_0 L_{\mathrm{eff}}/(1 + z^2/z_0^2)$, I_0 is the peak intensity of the

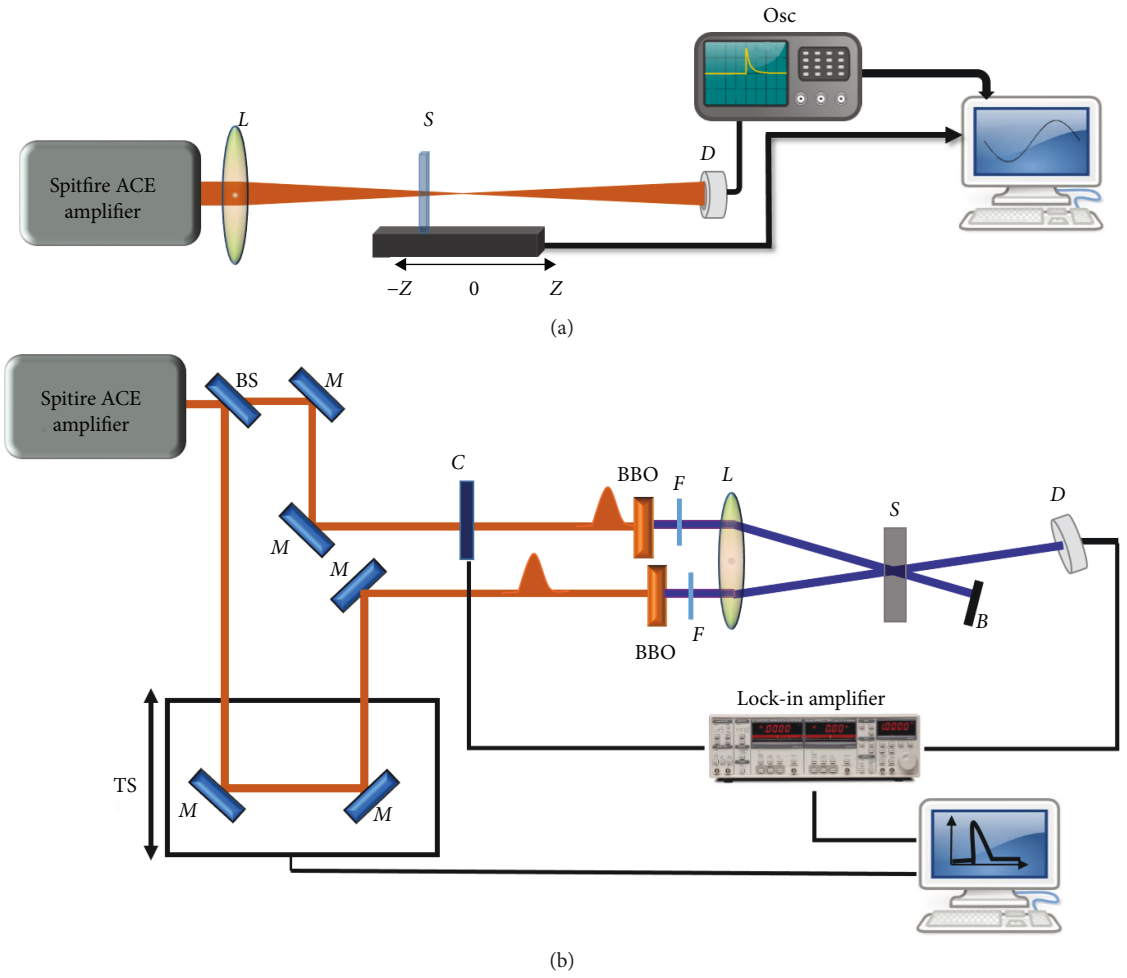

Figure 1: Experimental setup for (a) Z-scan technique and (b) transient absorption. M: reflecting mirror; BS: beam splitter; TS: translational stage; L: lens; C: mechanical optical chopper; S: sample cuvette; D: photodiode; B: beam blocker; BBO: beta barium borate crystal; F: filter; Osc: oscilloscope.

laser pulse, I_{sat} is the saturation intensity of the optically active medium which depends on the concentration of the medium, z_0 is the Rayleigh length defined as $z_0 = k(w_0^2)/2$, ω_0 is the radius of the focused beam, $L_{eff} = [1 - \exp(-\alpha_0 L)]/\alpha_0$ is the effective length of the medium, and α_0 is the linear absorption coefficient of the medium.

2.3. TA Measurements. A conventional noncollinear degenerate pump-probe technique was employed to observe the transient absorption (TA) in chemically prepared Ag NP in deionized water at different temperatures. Schematic of TA setup is shown in Figure 1(b). The commercially available regenerative amplifier (Spitfire ACE, Spectra-Physics, 800 nm, 1 kHz) was used as a source for the femtosecond pulses for the TA study. TA studies were performed at resonant 400 nm obtained by doubling of the fundamental laser pulse at 800 nm from the amplifier using a nonlinear crystal (BBO). The laser pulse from the amplifier was split into two pulses using a 70-30 beamsplitter. One pulse was used as a pump, and another pulse was used as a probe, which was passed through the motorized delay line to control the time separation between the pump and probe pulses. The relative intensity and a beam diameter of the pump and the probe pulse were adjusted to be ~20 : 1 and ~1 : 2, respectively, to fulfill the condition required for the pump-probe experiment. Pump pulse power of 20 nJ was used for the TA study for all measurements. The pulse width of the laser pulse from the amplifier was found to be 35 fs, which was measured at the sample position using 0.2 mm BBO crystal. The measured pulse width was further confirmed by measuring it using a commercially available autocorrelator. The arrival time of probe pulses with respect to pump pulses was controlled by moving the motorized translational stage connected to the motion controller. An ultrafast photodiode (model: DET025AL, Thorlabs, China) connected to a lock-in amplifier was used to measure the transmittance of the probe pulse with respect to the position of the motorized stage. The lock-in amplifier was externally triggered with an optical chopper running at 300 Hz.

3. Result and Discussion

3.1. Linear and Nonlinear Optical Properties of Chemically Prepared Ag NPs. The optical absorption spectra of Ag NP

suspensions in deionized water were measured using a UV-Visible spectrophotometer (Agilent Technologies). From Figure 2, we can observe distinctive surface plasmon resonance at 389 nm for S1 and S3, 381 nm for S5 and S7, and 385 nm for S9 and S11. The emergence of these peaks was the direct consequence of the size of Ag NPs. The SPRs of Ag NPs prepared at 0°C exhibit an absorption band at 389 nm with a side absorption band at 433 nm. These absorption peaks around 390 nm in all Ag NPs are the result of direct transition from occupied sp to unoccupied sp [32]. Our observation shows the emergence of the absorption band at 430 nm in prepared Ag NPs at 0°C and 25°C whereas the emergence of the absorption peak at 350 nm was observed at 60°C. The emergence of these absorption bands can be attributed to the Ag NP distortion which results in the formation of prolate and oblate spheroid NPs. These distorted NPs are responsible for the emergence of the SPR band at 350 and 430 nm due to the high multipolar excitation [46]. SEM images and their respective histograms of prepared Ag NPs at different temperatures are shown in Figures 3(a)–3(f). It is evident from the SEM images that the shape of the prepared Ag NPs is distorted. Size and its distribution of Ag NPs associated with S3, S7, and S11 are observed to be similar and narrow as compared to S1, S5, and S9, respectively. As mentioned in the experimental setup, S1, S5, and S9 were prepared using slow addition of aqueous $AgNO_3$ in aqueous SBH solution. The mechanism of creation of NPs involves the reduction of metal ions by a reducing agent which is followed by the nucleation process of clustering for reduced metal that acts as a seed to grow the different sizes of NPs. At first, the smaller-sized aggregates are mostly formed under the dripping method of addition. These aggregates grow in bigger-size NPs upon further addition of metal ions in the suspension. This process leads to the bigger-sized NPs compared to NPs prepared by mixing metal ion and reducing agent instantaneously, where the nucleation is the limiting process for the formation of NPs.

NLO properties of chemically prepared Ag NPs in deionized water were investigated using the Z-scan technique with amplified femtosecond pulses at resonant 400 nm and nonresonant 800 nm. Prior to the Z-scan measurement, the open aperture was measured for deionized water, which exhibits negligible optical nonlinearity with a maximal applied peak intensity of 1.2×10^{11} W cm^{-2} at 400 nm and 2.5×10^{11} W cm^{-2} at 800 nm. Figure 4 shows the open aperture trace of all NPs (S1, S3, S5, S7, S9, and S11) at the peak pulse intensity of 9×10^{10} W cm^{-2} at 400 nm. As shown in Figure 4, all prepared Ag NPs show the increase in the transmittance of 400 nm wavelength as the sample approaches the focal point, which indicates that all materials exhibit SA at 400 nm. We analyzed the OA Z-scan data by fitting the standard transmittance equation (equation 1) of SA. The estimated values of I_{sat} were tabulated in Table 1 for respective NP suspension. The saturable absorption behaviors for all NP suspension can be explained by the presence of SPR resonance at 400 nm which resulted in the increase of transmittance through Ag NP suspensions.

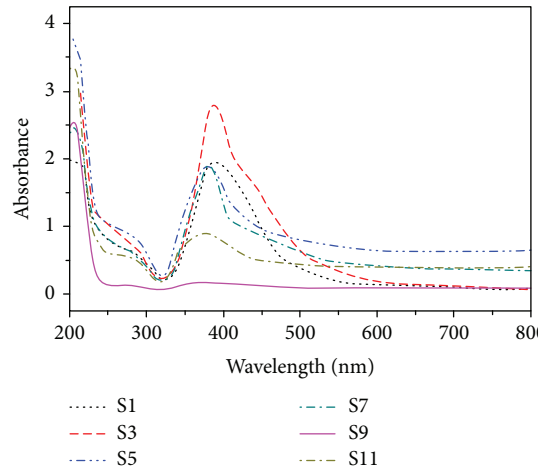

Figure 2: Optical absorption spectra of chemically prepared NPs in deionized water.

Ag NPs exhibit an intense absorption band at ~400 nm due to sp → sp transition in Ag which highly depends on the size of the Ag NPs [25, 47]. At the employed peak intensity of femtosecond pulses, the intraband sp → sp transitions are possible. As the pulse energy at resonant 400 nm further increases, the d → sp transition can also occur through excitation of electrons from the occupied d state to unoccupied sp state which can open the channel for two-photon absorption shown in scheme (2) of Figure 5. Similarly, in addition to the d-sp transition, interband two-photon absorption at 400 nm is also possible via occupied sp to unoccupied sp band (sp → sp transition) shown in scheme (3) of Figure 5. The excitation of Ag NPs with 400 nm is considered as high energy photon absorption at a resonant wavelength which can lead to the equalization of electron population in occupied and unoccupied energy levels. Thus, the absorption saturation is evident at 400 nm which is the case for samples S1 to S11, and the mechanism is depicted in scheme (1) of Figure 5.

Figure 6 shows the open aperture Z-scan at 800 for each Ag NPs. Similar to the Z-scan profile at 400 nm, S1, S3, S5, and S7 exhibit absorption saturation with I_{sat} of 330×10^{10} W cm^{-2}, 21×10^{10} W cm^{-2}, 1.9×10^{10} W cm^{-2}, and 3.1×10^{10} W cm^{-2}, respectively. On the other hand, S9 and S11 exhibit reverse saturable absorption in addition to absorption saturation at an employed peak intensity of 2.7×10^{11} W c m^{-2}. In order to fit the Z-scan profile for S9 and S11, a combination of equation 1 and equation 2 was used. The estimated value of I_{sat} and β are 83×10^{10} W cm^{-2} and 1.7×10^{-11} cm^{-1} W for S9 and 27×10^{10} W cm^{-2} and 4.6×10^{-11} cm^{-1} W for S11. These profiles can be explained with scheme (4) of Figure 5 for absorption saturation in S1 to S7 and schemes (4) and (5) of Figure 5 for the explanation of S9 and S11. Under the high-intensity regime at 800 nm, the electronic excitation takes place via intraband sp → sp transition as shown in scheme (4) of Figure 5. Thus, the increase in the transmittance at 800 nm was observed for S1 to S7, whereas a

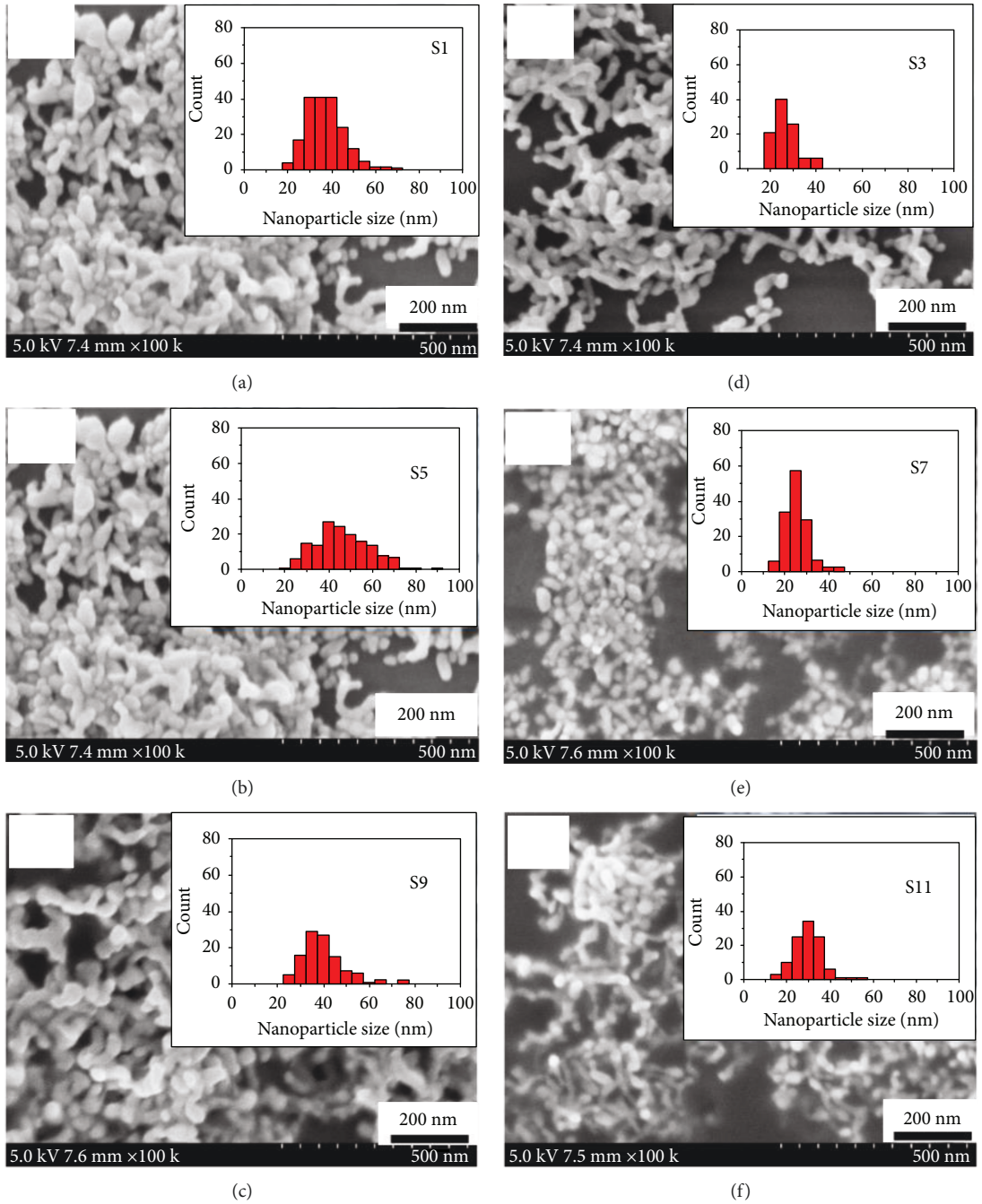

FIGURE 3: SEM image of chemically prepared Ag NPs in deionized water by dripping aqueous $AgNO_3$ in SBH slowly at (a) 0°C, (b) 25°C, and (c) 60°C, whereas (d) 0°C, (e) 25°C, and (f) 60°C represent the Ag NPs prepared by mixing aqueous $AgNO_3$ and SBH instantaneously.

completely different scenario was observed where simultaneous absorption of two-photon at 800 resulting in the intraband transition from sp → sp was observed as shown in scheme (5) of Figure 5. This results in the decrease in the transmittance as the sample further moves toward the focus indicating the combined ramification of SA and TPA processes. Recently, several groups have measured the NLO properties of the Ag NPs with various laser pulse widths [26, 48, 49]. Particularly, the comparison of the application of 200 ps and 60 fs pulses, which clearly depict the effect of long pulses on the NLO properties of NPs, has been reported in [48]. These studies were mostly carried out using the average particle size of 13 nm. Present studies were performed using the average particle sizes ranging from 25 to 38 nm.

We have also measured the NLO response of prepared Ag NPs with 30 times lower concentration at 400 nm. At a resonant wavelength of 400 nm with a low concentration of Ag NPs, the RSA was observed with absorption saturation (see Figure 7). Thus, the obtained profile was fitted with a combination of SA and TPA as mentioned in equation 1 and equation 2. The estimated values of I_{sat} were 1.4×10^{11} W cm^{-2}, 1.1×10^{11} W cm^{-2}, 1.4×10^{11} W cm^{-2},

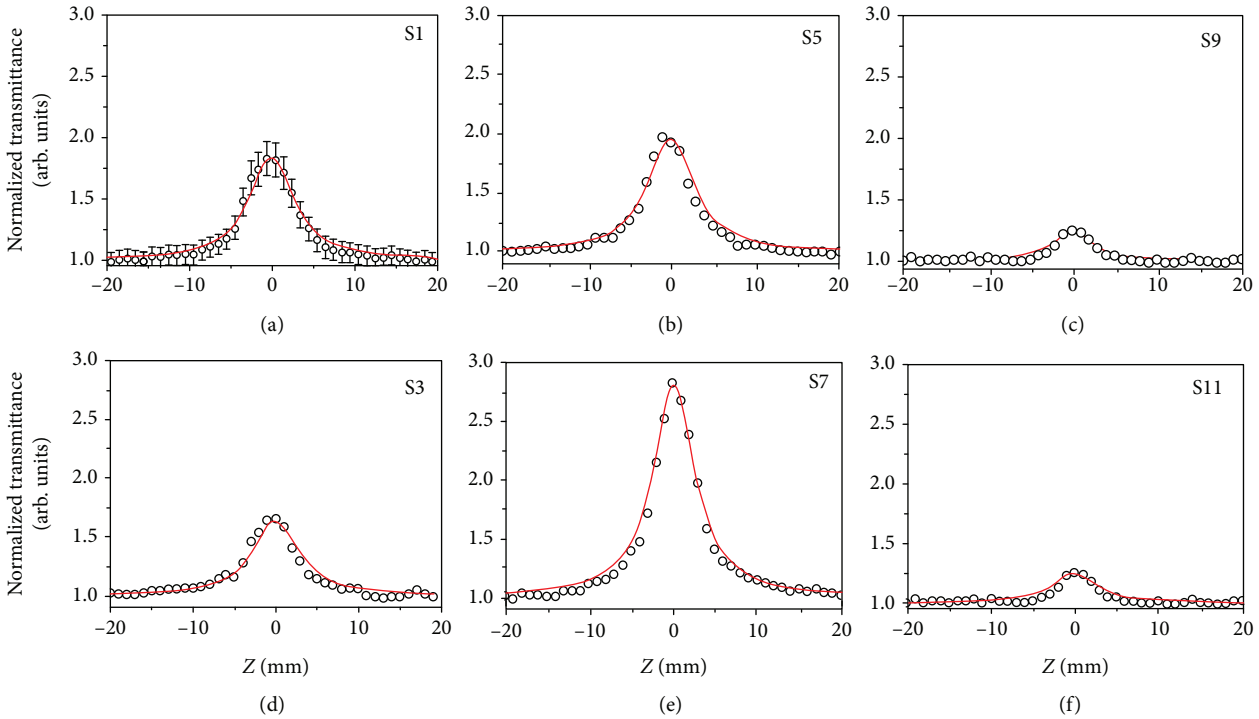

FIGURE 4: Open aperture Z-scan trace for chemically prepared Ag NPs with a peak intensity of 9.9×10^{10} W cm^{-2} at 400 nm. (a) S1, (b) S5, (c) S9, (d) S3, (e) S7, and (f) S11. The open circle represents the experimental data, and the solid line represents the theoretical fit.

TABLE 1: The NLO and decay time characteristics of chemically prepared Ag NPs in deionized water.

Sample	Particle size (nm)	Nonlinear absorption					Time constant			
		400 nm			800 nm		400 nm (high concentration)			
		High concentration	Low concentration		Low concentration					
		I_{sat} (10^{10} W cm^{-2})	I_{sat} (10^{11} W cm^{-2})	β (10^{-10} cm W^{-1})	I_{sat} (10^{10} W cm^{-2})	β (10^{-11} cm W^{-1})	τ_{th} (fs)	$\tau_{e\text{-}ph}$ (ps)	τ_{RBM} (ps)	f_{RBM} (THz)
S1	37	10 ± 1	1.4 ± 0.1	1.1 ± 0.2	330 ± 40	—	220 ± 20	2.3 ± 0.1	7 ± 1	181
S3	25	13 ± 2	1.1 ± 0.2	1.3 ± 0.1	21 ± 4	—	220 ± 20	1.8 ± 0.2	9 ± 3	198
S5	38	8.8 ± 1	1.4 ± 0.2	1.2 ± 0.2	1.9 ± 0.3	—	200 ± 20	1.5 ± 0.2	10 ± 3	166
S7	25	4.7 ± 1	1.3 ± 0.2	1.4 ± 0.2	3.1 ± 0.4	—	200 ± 20	1.8 ± 0.2	12 ± 2	200
S9	30	34 ± 4	1.4 ± 0.2	1.1 ± 0.2	83 ± 6	1.7 ± 4	200 ± 30	2.1 ± 0.4	—	—
S11	37	34 ± 5	1.1 ± 0.2	1.3 ± 0.2	27 ± 4	4.6 ± 5	200 ± 30	1.4 ± 0.3	—	—

1.3×10^{11} W cm^{-2}, 1.3×10^{11} W cm^{-2}, and 1.1×10^{11} W cm^{-2} for S1, S3, S5, S7, S9, and S11, respectively, whereas the corresponding β values were 1.1×10^{-10} cm W^{-1}, 1.3×10^{-10} cm W^{-1}, 1.2×10^{-10} cm W^{-1}, 1.4×10^{-10} cm W^{-1}, 1.1×10^{-10} cm W^{-1}, and 1.3×10^{-10} cm W^{-1} for S1, S3, S5, S7, S9, and S11, respectively. These nonlinear optical properties were considered to be affected by electronic excitation schemes (2) and (3) in addition to scheme (1) of Figure 5. Under this condition, in addition to the saturable absorption at high intensity, the TPA process can occur either via interband d → sp transition or via intraband sp → sp transition. This leads to a decrease in the transmittance as the sample moves toward the focus.

It was observed that the RSA value is higher for S7 compared to other NPs which can be attributed to the smaller size of Ag NPs. It is evident from the calculated value of I_{SA} and β that I_{SA} decreases and β increases as the sizes of the Ag NPs increase as shown in Figure 8. It was observed that under resonant excitation SA can dominate over RSA. Various reports have shown the role of concentration in SA over RSA processes [50]. The result mentioned in this work was compared with the earlier work reported by us [49] where the dependence of the pulse width of the laser pulses on the NLO properties of chemically prepared NPs was investigated. The nonlinear absorption characteristics for Ag NPs at 800 nm in this work were found to be consistent with the

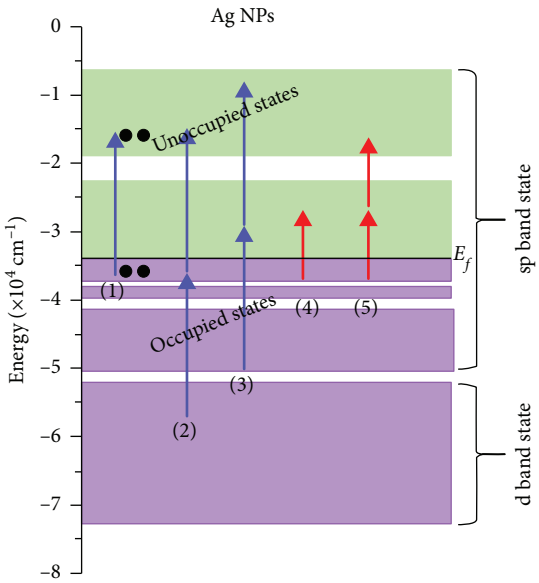

FIGURE 5: Schematic of the energy level diagram and electronic excitation for Ag NPs [25]. The equal population in the lower and upper electronic states represents the absorption saturation represented by black circular dots. The blue-colored upward arrow represents excitation using 400 nm (3.1 eV) whereas the red-colored upward arrow represents 800 nm (1.55 eV) excitation. E_f corresponds to the energy associated with the Fermi level in cm^{-1}.

previous report. The estimated values of nonlinear absorption for all samples are represented in Table 1.

3.2. Pump-Probe Study of Chemically Prepared Ag NP Suspensions. We have performed the degenerate pump-probe measurement of the chemically prepared Ag NPs in deionized water at 400 nm with 35 fs pulses. The intensities of the pump and probe pulses were 17 GW cm^{-2} and 1 GW cm^{-2}, respectively. Here, all NP suspensions exhibit photobleaching effect evident of saturable absorption as shown in Z-scan profile of Ag NPs at 400 nm. Figure 9 shows the temporal evolution of change in transmittance of probe pulses. In pump-probe experiments, the electron distribution in the particle is perturbed by femtosecond pump pulses which were probed by a time-delayed weak pulse either at the resonant wavelength or close to the resonant wavelength [51–53]. The energy relaxation upon excitation from pump pulses is generally described as a series of relaxation processes which include electron-electron scattering, electron-phonon coupling, and heat dissipation through the surrounding. Apart from these relaxation processes, the particle can go under acoustic vibrations through two distinct excitation mechanisms. First is the creation of pressure on the surface of the particle due to a sudden surge in electron temperature [54], and second is the energy transfer from the electron to the lattice leading to the increase in the equilibrium interatomic distance by thermal expansion [55]. The acoustic vibration time scale is longer than the electron-lattice relaxation time. Thus, the particles are brought out of equilibrium leading to the mechanical oscillations which are responsible for the periodic change in size and shape of NPs. These periodic oscillations are easy to probe by a wavelength closer to plasmonic resonance. In particles, the fundamental mode of vibration involves the radial breathing mode (RBM) which depends on both bulk and searing elastic moduli of metal.

In chemically prepared Ag NPs, distinct damped oscillation in probe pulse transmittance was observed for S1, S3, S5, and S7 due to acoustic vibration, which is superposed with the exponentially decaying back of the excited Ag NPs to its ground state through cooling of the hot lattice. However, this acoustic vibration was not observed for S9 and S11. As seen in Figures 9(e) and 9(f)), the signal to noise ratio is poor as compared to the other transmission profiles which can be directly correlated with the impact of the low concentration of the Ag NPs in S9 and S11. The damping in the acoustic vibration was witnessed which is associated with the damping time of the breathing mode due to the effect of the surrounding solvent. These oscillations were observed within 20 ps after the 0-time delay between pump and probe pulses. Thus, in order to obtain the relaxation time constant and damping time of the vibrations, we fitted the obtained decay profile with the exponential decay equation represented in equation 3, which contains the electron thermalization (τ_{th}) and electron-phonon (e-ph) coupling (τ_2) time constants, whereas the characteristic time constant associated with RBM (τ_{RBM}) and frequency (ν) associated with oscillations is expressed in equation 4:

$$\Delta T/T = A_1 \exp\left(-t/\tau_{\text{th}}\right) + A_2 \exp\left(-t/\tau_{\text{e-ph}}\right), \tag{3}$$

$$[\Delta T/T]_{\text{Residual}} = A_0 \exp\left(-t/\tau_{\text{RBM}}\right) \cos\left(2\pi f_{\text{RBM}} t - \phi_b\right), \tag{4}$$

where A_1, A_2, A_0, and ϕ_b are proportionality constants associated with three decay times and phase. In order to determine the time constant associated with Ag NPs, the obtained TA profile was first fitted with equation 3, which yields the time constant associated with electron thermalization and electro-phonon interaction. The residual of the fitted data with equation 3 was fitted with equation 4 to obtain the RBM frequency and the damping time constant. Figure 10 shows the fitting of the residual $[\Delta T/T]$ with equation (4) for S1, S3, S5, and S7. The obtained lifetime (τ_{th}) associated with Ag NPs was found to be 220 fs for S1 and S3 and 200 fs for S5, S7, S9, and S11, respectively. These time constants can be attributed to the electron thermalization. The τ_{th} reflects the energy redistribution inside the electron cloud after absorption of a femtosecond pulse, which is generally determined by the electron-electron scattering process with certain energy range taking place alongside slow processes. The time constants ($\tau_{\text{e-ph}}$) associated with Ag NPs were 2.3 ps for S1, 1.8 ps for S3, 1.5 ps for S5, 1.8 ps for S7, 2.1 ps for S9, and 1.4 ps for S11. However, the damping time constant (τ_{RBM}) associated with the radial breathing mode was found to be 7 ps for S1, 9 ps for S3, 10 ps for S5, and 12 ps for S7 with their respective RBM frequencies of 181 Hz for S1, 198 Hz for S3, 166 Hz for S5, and 200 Hz for S7. These results were presented in Table 1 for their better understanding. This damping

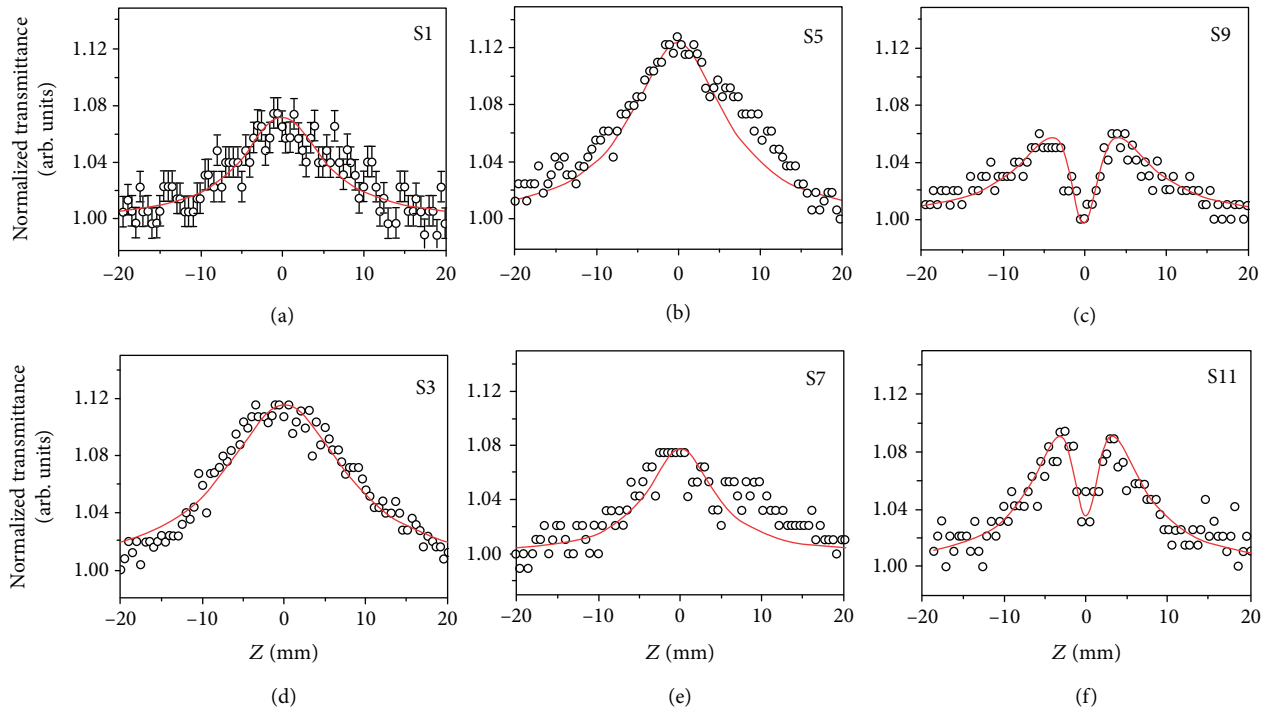

FIGURE 6: Open aperture Z-scan trace for chemically prepared Ag NPs with a peak intensity of 2.7×10^{11} W cm^{-2} at 800 nm. (a) S1, (b) S5, (c) S9, (d) S3, (e) S7, and (f) S11. The open circle represents the experimental data, and the solid line represents the theoretical fit.

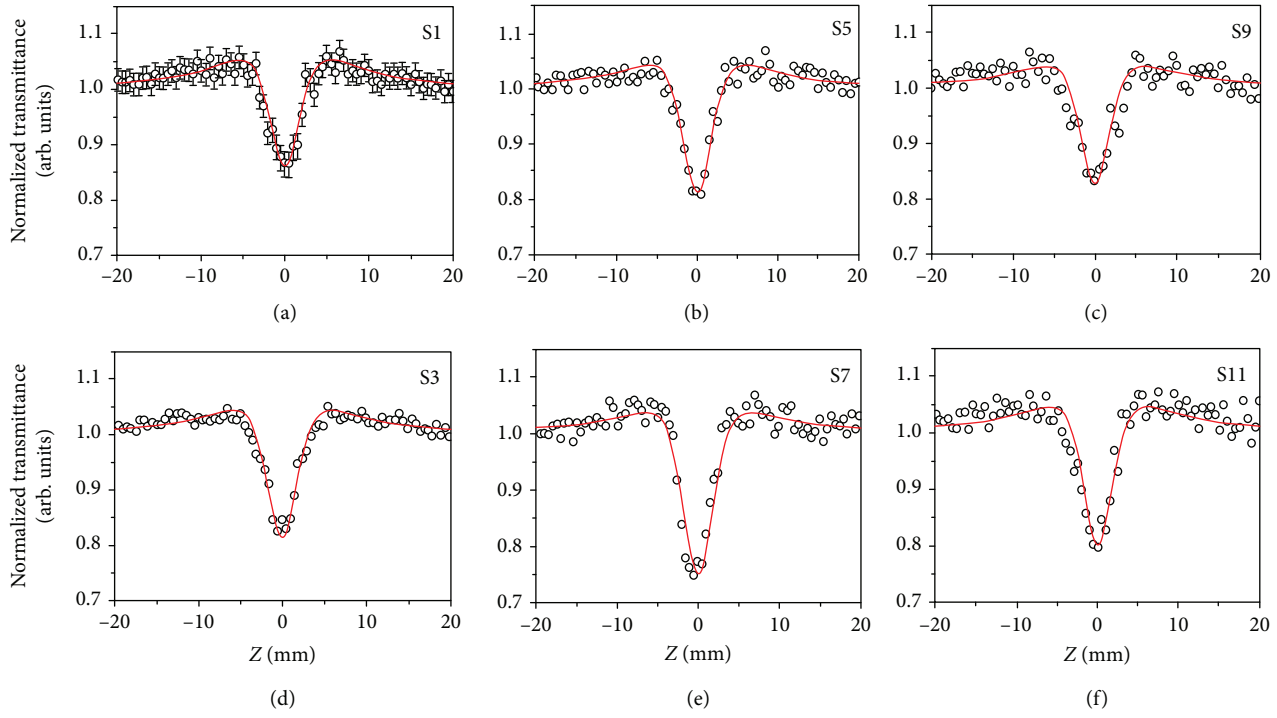

FIGURE 7: Open aperture Z-scan trace for chemically prepared Ag NPs at low concentration with a peak intensity of 1.2×10^{11} W cm^{-2} at 400 nm. (a) S1, (b) S5, (c) S9, (d) S3, (e) S7, and (f) S11. The open circle represents the experimental data, and the solid line represents the theoretical fit.

time constant can be attributed to the homogeneous damping time which is mostly governed by the relationship, $\tau_{\mathrm{RBM}} = 2.9R/v_L$, where R is the radius of NPs and v_L is the longitudinal sound velocity in NPs. There have been several reports on the effect of size of the gold NPs on RBM frequency [54] which shows that with an increase

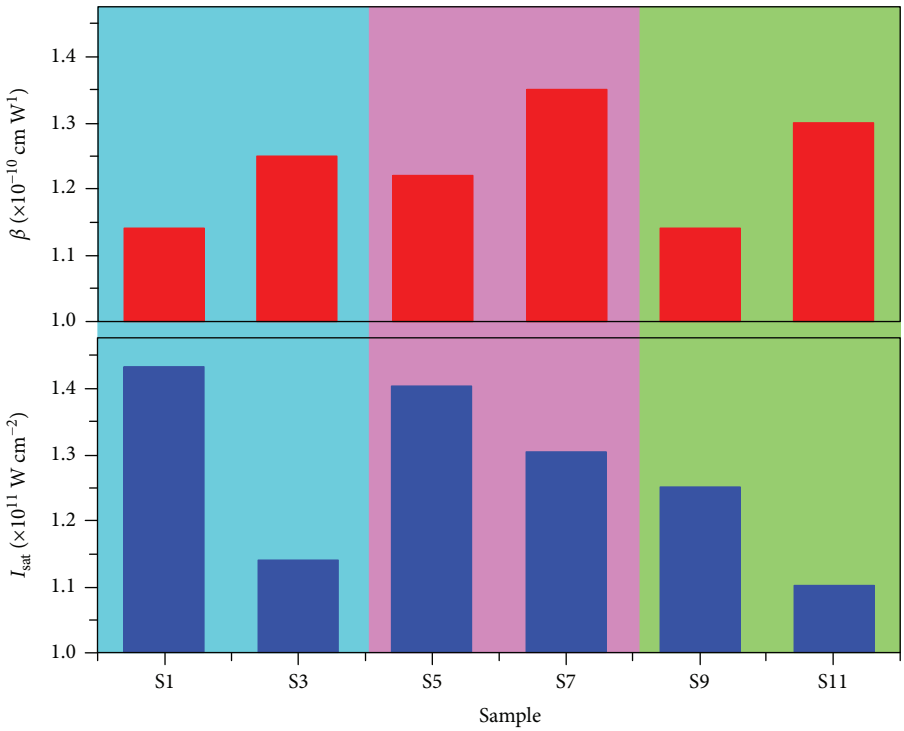

FIGURE 8: Comparison of I_{sat} and RSA coefficient of all prepared Ag NPs at 400 nm femtosecond laser pulses.

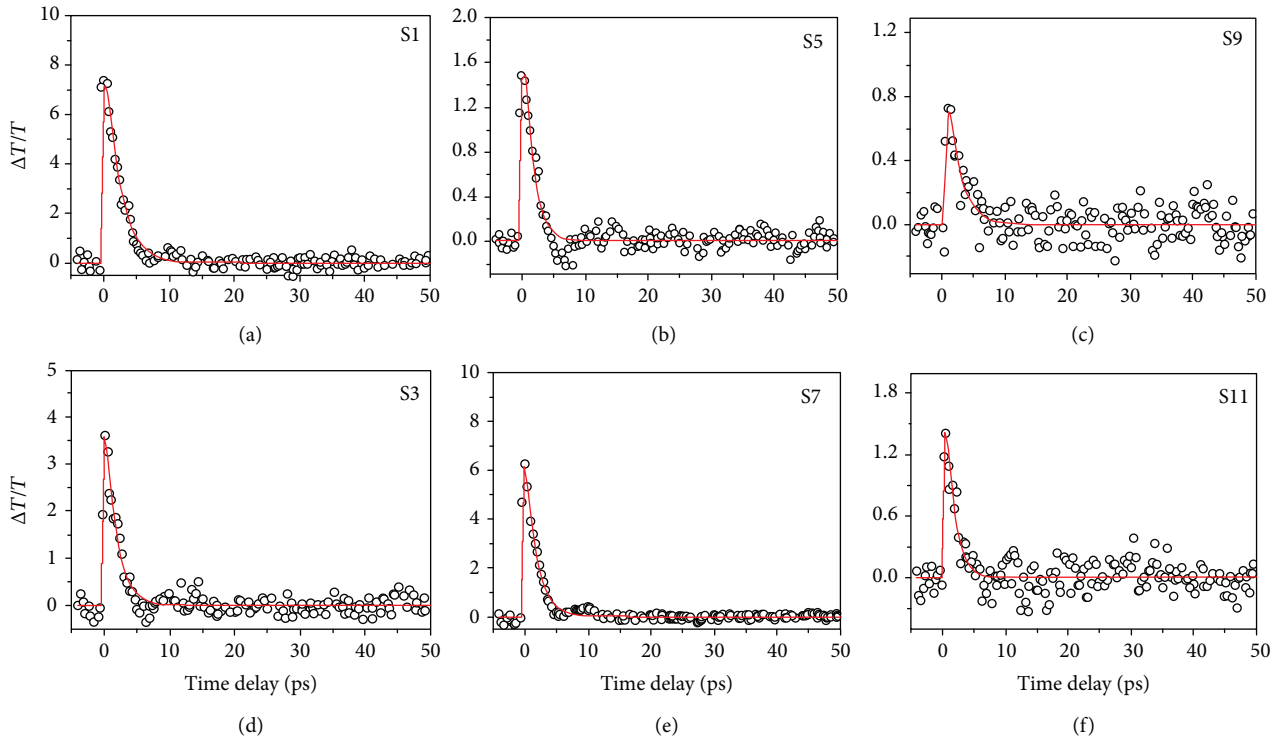

FIGURE 9: TA profile of chemically prepared Ag NPs: (a) S1, (b) S5, (c) S9, (d) S3, (e) S7, and (f) S11 NPs at 400 nm. The open circle represents the experimental data, and the solid line represents the theoretical fit.

in the size of NPs, RBM frequency decreases due to the influence of the surrounding medium. There are few reports on the RBM mode lifetime for Ag NPs [56, 57] which were observed in the glass matrix at the temperature of 80 K. It was shown that the obtained RBM lifetime is longer as compared to the theoretically predicted values, whereas in the present paper, we have performed the measurements at room temperature, which resulted in the

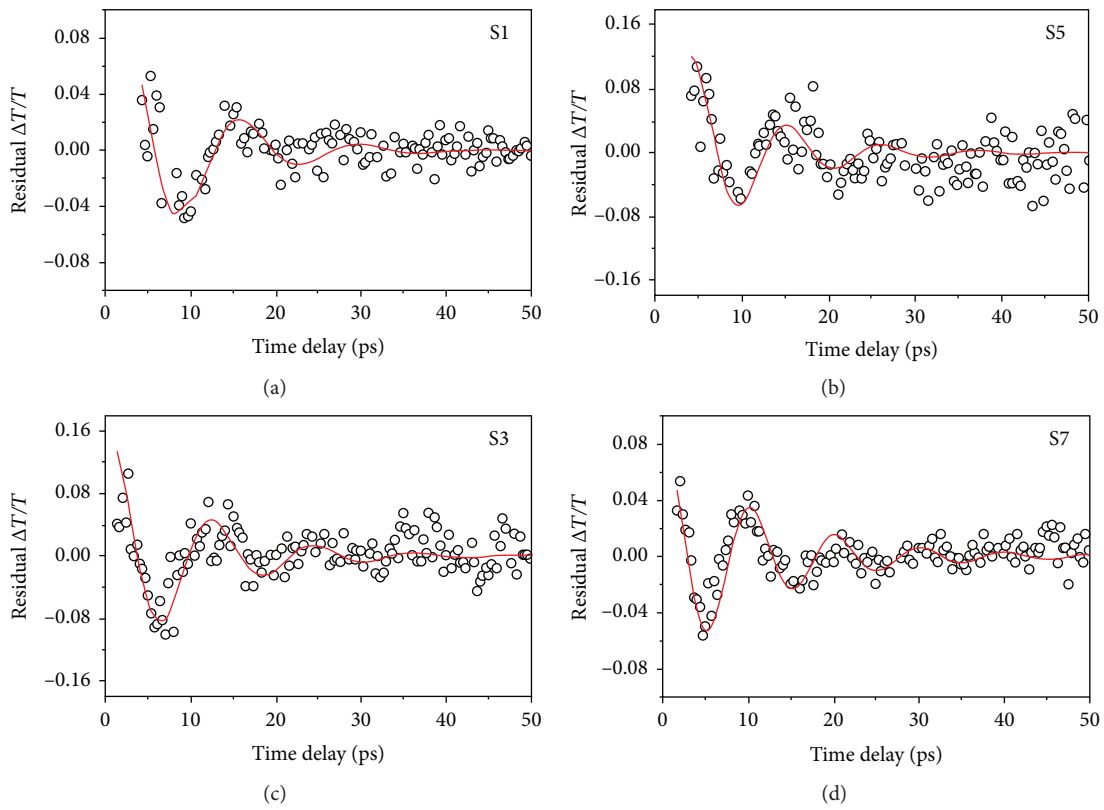

FIGURE 10: Residual of fit from equation 3 for chemically prepared Ag NPs (a) S1, (b) S5, (c) S3, and (d) S7. The open circle represents the residual of experimental data from the fitting of equation 3, and the solid line represents the theoretical fit.

shorter RBM lifetime as compared to the theoretical value. This difference could be due to the influence of the surrounding solvent and the temperature of the solvent bath.

4. Conclusions

In conclusion, we have reported the nonlinear optical response of chemically prepared Ag NPs in deionized water using femtosecond laser pulses at 400 nm and 800 nm. It was observed that the size of Ag NPs can have a large influence on NLO probability. The smaller-size Ag NPs have shown large RSA coefficient (β) and small SA intensity. These absorption saturations can be attributed to the intraband sp → sp transition in Ag NPs whereas interband d-sp or intraband sp-sp transition is responsible for the RSA process which clearly explains the observed intensity profile in our Z-scan measurements. This study shows that saturable absorption has a dominating factor for a higher concentration of Ag NPs over the RSA process at resonance excitation. It is evident from the nonlinear optical characterization of Ag NPs that there is a correlation between SA and RSA. It is observed that Ag NP processing low I_{sat} have large RSA probabilities.

The time-resolved studies of Ag NPs at 400 nm show ~200 fs and 1.5-2.3 ps dynamics, which is attributed to the electron thermalization and electron-phonon relaxation process. Ultrafast dynamics also reveals the damped oscillation in Ag NPs associated with acoustic vibration at the excitation wavelength of 400 nm. Under our experimental condition, we observed the RBM vibration in prepared Ag NPs which depends on the size of NPs. These RBM vibrations have the decay time in picosecond which also depends on the size of NPs and the surrounding environments.

Data Availability

The data used to support the findings of this study are available from the corresponding author upon request.

Conflicts of Interest

The authors declare that they have no conflicts of interest.

Acknowledgments

The financial support from the National Key Research and Development Program of China (2018YFB1107202 and 2017YFB1104700), the National Natural Science Foundation of China (91750205, 61774155, and 11774340), the Jilin Provincial Science and Technology Development Project (20180414019GH), and The Key Program of the International Partnership Program of CAS (181722KYSB20160015) is appreciated. R.A.G. thanks the financial support from the Chinese Academy of Sciences President's International Fellowship Initiative (Grant No. 2018VSA0001).

References

[1] P. Tartaj, M. a. del Puerto Morales, S. Veintemillas-Verdaguer, T. gonz Lez-Carre o, and C. J. Serna, "The preparation of magnetic nanoparticles for applications in biomedicine," *Journal of Physics D: Applied Physics*, vol. 36, no. 13, pp. R182–R197, 2003.

[2] J. J. Giner-Casares, M. Henriksen-Lacey, M. Coronado-Puchau, and L. M. Liz-Marzán, "Inorganic nanoparticles for biomedicine: where materials scientists meet medical research," *Materials Today*, vol. 19, no. 1, pp. 19–28, 2016.

[3] N. T. K. Thanh and L. A. W. Green, "Functionalisation of nanoparticles for biomedical applications," *Nano Today*, vol. 5, no. 3, pp. 213–230, 2010.

[4] W. P. McConnell, J. P. Novak, L. C. Brousseau, R. R. Fuierer, R. C. Tenent, and D. L. Feldheim, "Electronic and optical properties of chemically modified metal nanoparticles and molecularly bridged nanoparticle arrays," *Journal of Physical Chemistry B*, vol. 104, no. 38, pp. 8925–8930, 2000.

[5] M. Williams, A. Villarreal, K. Bozhilov, S. Lin, and P. Talbot, "Metal and silicate particles including nanoparticles are present in electronic cigarette cartomizer fluid and aerosol," *PLoS One*, vol. 8, no. 3, article e57987, 2013.

[6] H. Ditlbacher, J. R. Krenn, B. Lamprecht, A. Leitner, and F. R. Aussenegg, "Spectrally coded optical data storage by metal nanoparticles," *Optics Letters*, vol. 25, no. 8, pp. 563–565, 2000.

[7] J.-S. Lee, "Recent progress in gold nanoparticle-based non-volatile memory devices," *Gold Bulletin*, vol. 43, no. 3, pp. 189–199, 2010.

[8] K.-S. Lee and M. A. El-Sayed, "Gold and silver nanoparticles in sensing and imaging: sensitivity of plasmon response to size, shape, and metal composition," *Journal of Physical Chemistry B*, vol. 110, no. 39, pp. 19220–19225, 2006.

[9] G. Doria, J. Conde, B. Veigas et al., "Noble metal nanoparticles for biosensing applications," *Sensors*, vol. 12, no. 2, pp. 1657–1687, 2012.

[10] X. Luo, A. Morrin, A. . J. Killard, and M. . R. Smyth, "Application of nanoparticles in electrochemical sensors and biosensors," *Electroanalysis*, vol. 18, no. 4, pp. 319–326, 2006.

[11] K. Furusawa, K. Takahashi, H. Kumagai, K. Midorikawa, and M. Obara, "Ablation characteristics of Au, Ag, and Cu metals using a femtosecond Ti: sapphire laser," *Applied Physics*, vol. 69, no. 7, Supplementary 1, pp. S359–S366, 1999.

[12] R. Rangel-Rojo, J. McCarthy, H. T. Bookey et al., "Anisotropy in the nonlinear absorption of elongated silver nanoparticles in silica, probed by femtosecond pulses," *Optics Communications*, vol. 282, no. 9, pp. 1909–1912, 2009.

[13] S. Qu, Y. Zhang, H. Li, J. Qiu, and C. Zhu, "Nanosecond nonlinear absorption in Au and Ag nanoparticles precipitated glasses induced by a femtosecond laser," *Optical Materials*, vol. 28, no. 3, pp. 259–265, 2006.

[14] Q.-Q. Wang, J.-B. Han, H.-M. Gong et al., "Linear and nonlinear optical properties of Ag nanowire polarizing glass," *Advanced Functional Materials*, vol. 16, no. 18, pp. 2405–2408, 2006.

[15] R. A. Ganeev, A. I. Ryasnyansky, A. L. Stepanov, and T. Usmanov, "Nonlinear optical susceptibilities of copper- and silver-doped silicate glasses in the ultraviolet range," *Physica Status Solidi B*, vol. 238, no. 2, pp. R5–R7, 2003.

[16] Y. Gao, W. Wu, D. Kong, L. Ran, Q. Chang, and H. Ye, "Femtosecond nonlinear absorption of Ag nanoparticles at surface plasmon resonance," *Physica E: Low-dimensional Systems and Nanostructures*, vol. 45, pp. 162–165, 2012.

[17] C. Zheng, W. Li, W. Chen, and X. Ye, "Nonlinear optical behavior of silver nanopentagons," *Materials Letters*, vol. 116, pp. 1–4, 2014.

[18] B.-H. Yu, D.-L. Zhang, Y.-B. Li, and Q.-B. Tang, "Nonlinear optical behaviors in a silver nanoparticle array at different wavelengths," *Chinese Physics B*, vol. 22, no. 1, article 014212, 2013.

[19] J. Jayabalan, A. Singh, R. Chari, and S. M. Oak, "Ultrafast third-order nonlinearity of silver nanospheres and nanodiscs," *Nanotechnology*, vol. 18, no. 31, article 315704, 2007.

[20] M. Hari, S. Mathew, B. Nithyaja, S. A. Joseph, V. P. N. Nampoori, and P. Radhakrishnan, "Saturable and reverse saturable absorption in aqueous silver nanoparticles at off-resonant wavelength," *Optical and Quantum Electronics*, vol. 43, no. 1-5, pp. 49–58, 2012.

[21] A. Ajami, W. Husinsky, B. Svecova, S. Vytykacova, and P. Nekvindova, "Saturable absorption of silver nanoparticles in glass for femtosecond laser pulses at 400nm," *Journal of Non-Crystalline Solids*, vol. 426, pp. 159–163, 2015.

[22] Y.-X. Zhang and Y.-H. Wang, "Nonlinear optical properties of metal nanoparticles: a review," *RSC Advances*, vol. 7, no. 71, pp. 45129–45144, 2017.

[23] H. H. Mai, V. E. Kaydashev, V. K. Tikhomirov et al., "Nonlinear optical properties of Ag nanoclusters and nanoparticles dispersed in a glass host," *Journal of Physical Chemistry C*, vol. 118, no. 29, pp. 15995–16002, 2014.

[24] U. Gurudas, E. Brooks, D. M. Bubb, S. Heiroth, T. Lippert, and A. Wokaun, "Saturable and reverse saturable absorption in silver nanodots at 532 nm using picosecond laser pulses," *Journal of Applied Physics*, vol. 104, no. 7, article 073107, 2008.

[25] R. Philip, P. Chantharasupawong, H. Qian, R. Jin, and J. Thomas, "Evolution of nonlinear optical properties: from gold atomic clusters to plasmonic nanocrystals," *Nano Letters*, vol. 12, no. 9, pp. 4661–4667, 2012.

[26] G. S. Boltaev, R. A. Ganeev, P. S. Krishnendu et al., "Strong third-order optical nonlinearities of Ag nanoparticles synthesized by laser ablation of bulk silver in water and air," *Applied Physics A*, vol. 124, no. 11, p. 766, 2018.

[27] R. van Leeuwen, "First-principles approach to the electron-phonon interaction," *Physics Review B*, vol. 69, no. 11, article 115110, 2004.

[28] G. Grimvall, *The Electron-Phonon Interaction in Metals*, North-Holland Publishing Co, Amsterdam, 1981.

[29] L. J. Sham and J. M. Ziman, "The electron-phonon interaction," *Solid State Physics*, vol. 15, pp. 221–298, 1963.

[30] G. V. Hartland, "Optical studies of dynamics in noble metal nanostructures," *Chemical Reviews*, vol. 111, no. 6, pp. 3858–3887, 2011.

[31] M. Galperin, M. A. Ratner, and A. Nitzan, "Molecular transport junctions: vibrational effects," *Journal of Physics: Condensed Matter*, vol. 19, no. 10, article 103201, 2007.

[32] C. Voisin, D. Christofilos, N. Del Fatti, and F. Vallée, "Femtosecond surface plasmon resonance dynamics and electron-electron interactions in silver nanoparticles," *The European Physical Journal D*, vol. 16, no. 1, pp. 139–144, 2001.

[33] M. Pelton, J. E. Sader, J. Burgin, M. Liu, P. Guyot-Sionnest, and D. Gosztola, "Damping of acoustic vibrations in gold nanoparticles," *Nature Nanotechnology*, vol. 4, no. 8, pp. 492–495, 2009.

[34] J. Conde, J. Rosa, J. C. Lima, and P. V. Baptista, "Nanophotonics for molecular diagnostics and therapy applications," *International Journal of Photoenergy*, vol. 2012, Article ID 619530, 11 pages, 2012.

[35] J. H. Son, B. Cho, S. Hong et al., "Ultrafast photonic PCR," *Light: Science & Applications*, vol. 4, no. 7, article e280, 2015.

[36] H. Ahmad, N. E. Ruslan, M. A. Ismail et al., "Silver nanoparticle-film based saturable absorber for passively Q-switched erbium-doped fiber laser (EDFL) in ring cavity configuration," *Laser Physics*, vol. 26, no. 9, article 095103, 2016.

[37] F. Guang-Hua, Q. Shi-Liang, G. Zhong-Yi, and W. Qiang, "Size-dependent nonlinear absorption and refraction of Ag nanoparticles excited by femtosecond lasers," *Chinese Physics B*, vol. 21, no. 4, article 047804, 2012.

[38] V. Liberman, M. Sworin, R. P. Kingsborough, G. P. Geurtsen, and M. Rothschild, "Nonlinear bleaching, absorption, and scattering of 532-nm-irradiated plasmonic nanoparticles," *Journal of Applied Physics*, vol. 113, no. 5, article 053107, 2013.

[39] N. Del Fatti, C. Voisin, D. Christofilos, F. Vallee, and C. Flytzanis, "Acoustic vibration of metal films and nanoparticles," *The Journal of Physical Chemistry A*, vol. 104, no. 18, pp. 4321–4326, 2000.

[40] A. Arbouet, N. Del Fattia, and F. Vallee, "Optical control of the coherent acoustic vibration of metal nanoparticles," *Journal Chemical Physical*, vol. 124, no. 14, article 144701, 2006.

[41] A. Crut, P. Maioli, N. Del Fatti, and F. Vallee, "Time-domain investigation of the acoustic vibrations of metal nanoparticles: size and encapsulation effects," *Ultrasonics*, vol. 56, pp. 98–108, 2015.

[42] M. A. Mahmoud, D. O'Neil, and M. A. El-Sayed, "Shape- and symmetry-dependent mechanical properties of metallic gold and silver on the nanoscale," *Nano Letters*, vol. 14, no. 2, pp. 743–748, 2014.

[43] W. Huang, W. Qian, and M. A. El-Sayed, "The optically detected coherent lattice oscillations in silver and gold monolayer periodic nanoprism arrays: the effect of interparticle coupling," *Journal of Physical Chemistry B*, vol. 109, no. 40, pp. 18881–18888, 2005.

[44] M. Sheik-Bahae, A. A. Said, and E. W. Van Stryland, "High sensitivity single-beam n_2 measurements," *Optics Letters*, vol. 14, no. 17, pp. 955–957, 1989.

[45] M. Sheik-Bahae, A. A. Said, T.-H. Wei, D. J. Hagan, and E. W. Van Stryland, "Sensitive measurement of optical nonlinearities using a single beam," *IEEE Journal of Quantum Electronics*, vol. 26, no. 4, pp. 760–769, 1990.

[46] I. O. Sosa, C. Noguez, and R. G. Barrera, "Optical properties of metal nanoparticles with arbitrary shapes," *The Journal of Physical Chemistry B*, vol. 107, no. 26, pp. 6269–6275, 2003.

[47] C. M. Aikens, S. Li, and G. C. Schatz, "From discrete electronic states to plasmons: TDDFT optical absorption properties of Ag_n (n=10, 20, 35, 56, 84, 120) tetrahedral clusters," *The Journal of Physical Chemistry C*, vol. 112, no. 30, pp. 11272–11279, 2008.

[48] G. K. Podagatlapalli, S. Hamad, S. P. Tewari, S. Sreedhar, M. D. Prasad, and S. V. Rao, "Silver nano-entities through ultrafast double ablation in aqueous media for surface-enhanced Raman scattering and photonics applications," *Journal of Applied Physics*, vol. 113, no. 7, article 073106, 2013.

[49] K. Zhang, R. A. Ganeev, K. S. Rao et al., "Interaction of pulses of different duration with chemically prepared silver nanoparticles: analysis of optical nonlinearities," *Journal of Nanomaterials*, vol. 2019, Article ID 6056528, 2 pages, 2019.

[50] Y. Fu, R. A. Ganeev, C. Zhao et al., "Ag_2S quantum dots in the fields of picosecond and femtosecond UV and IR pulses: optical limiting, nonlinear absorption and refraction properties," *Applied Physics B*, vol. 125, no. 1, 2019.

[51] J. H. Hodak, I. Martini, and G. V. Hartland, "Spectroscopy and dynamics of nanometer-sized noble metal particles," *Journal of Physical Chemistry B*, vol. 102, no. 36, article 6958, 6967 pages, 1998.

[52] J. Y. Bigot, V. Halte, J. C. Merle, and A. Daunois, "Electron dynamics in metallic nanoparticles," *Chemical Physics*, vol. 251, no. 1-3, pp. 181–203, 2000.

[53] C. Voisin, N. Del Fatti, D. Christofilos, and F. Vallée, "Ultrafast electron dynamics and optical nonlinearities in metal nanoparticles," *The Journal of Physical Chemistry B*, vol. 105, no. 12, pp. 2264–2280, 2001.

[54] M. Perner, S. Gresillon, J. März et al., "Observation of hot-electron pressure in the vibration dynamics of metal nanoparticles," *Physical Review Letters*, vol. 85, no. 4, pp. 792–795, 2000.

[55] G. V. Hartland, "Coherent vibrational motion in metal particles: determination of the vibrational amplitude and excitation mechanism," *Journal of Chemical Physics*, vol. 116, no. 18, pp. 8048–8055, 2002.

[56] E. Ghavanloo, S. A. Fazelzadeh, T. Murmu, and S. Adhikari, "Radial breathing-mode frequency of elastically confined spherical, nanoparticles subjected to circumferential magnetic field," *Physica E: Low-dimensional Systems and Nanostructures*, vol. 66, pp. 228–233, 2015.

[57] C. Voisin, N. Del Fatti, D. Christofilos, and F. Vallee, "Time-resolved investigation of the vibrational dynamics of metal nanoparticles," *Applied Surface Science*, vol. 164, no. 1-4, pp. 131–139, 2000.